Advances in Materials Physics and Chemistry, 2023, 13, 161-176
https://www.scirp.org/journal/ampc
ISSN Online: 2162-5328
ISSN Print: 2162-531X

A Novel Adsorbent Prepared by Aluminum-Containing Waste Residue and Its Application for Congo Red Wastewater Decolorization

Longfei Zhang[1], Xiaogang Han[2*], Jinxin Mu[2]

[1]College of Architecture and Civil Engineering, Kunming University, Kunming, China
[2]Changzhou Qingliu Environmental Protection Technology Co., Ltd., Changzhou, China
Email: *237414866@qq.com

How to cite this paper: Zhang, L.F., Han, X.G. and Mu, J.X. (2023) A Novel Adsorbent Prepared by Aluminum-Containing Waste Residue and Its Application for Congo Red Wastewater Decolorization. *Advances in Materials Physics and Chemistry*, **13**, 161-176.
https://doi.org/10.4236/ampc.2023.139012

Received: July 5, 2023
Accepted: September 19, 2023
Published: September 22, 2023

Abstract

Modified aluminum slag (MAS) was applied as an adsorbent for Congo red (CR) prepared by the hydrothermal treatment of $Ca(OH)_2$. At 25˚C, with a MAS dosage of 0.3 g, initial CR concentration of 100 mg/L and initial pH = 5, and the adsorption time was 40 min, the CR removal efficiency was 98.41%. The adsorption trend of CR conformed to the second-order kinetics, and the adsorption isotherm follows the Freundlich isotherm model. Compared with RAS, MAS has a larger pore volume and specific surface area. The mechanism of action of MAS on CR was the interaction between membrane diffusion and internal diffusion, and the adsorption rate during the membrane diffusion was the fastest.

Graphical Abstract

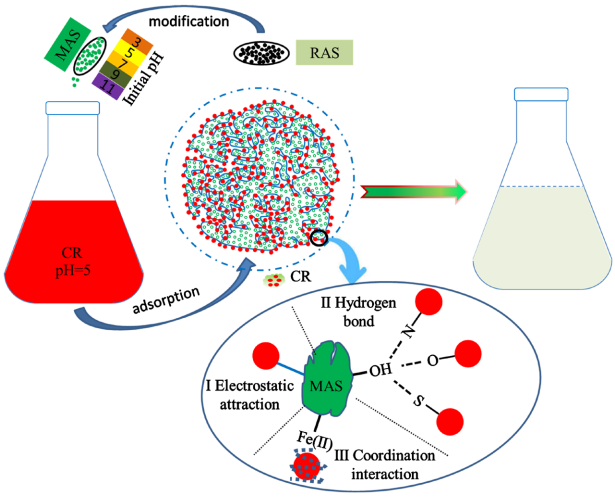

Keywords

Modified, Aluminum Containing Waste, Congo Red, Adsorption, Wastewater

1. Introduction

Organic dyes, widely used in cosmetics, printing and coloring agents, chemical reagents, etc., are major contributors to water pollution [1]. About 17% - 20% of industrial water pollution is caused by textile dyeing and processing [2]. Congo red (CR), a benzidine-direct azo anion dye, has a high loss rate during its production and application, and can easily enter the aquatic environment. Its formula is represented in **Figure 1**. In addition, CR produces more toxic aromatic amines under anaerobic microbial conditions, exacerbating environmental issues [3] [4] [5]. Therefore, it is usually treated with physical and chemical methods [6].

Raw aluminum slag (RAS), a waste product from the production of polyaluminum chloride, mainly consists of Al_2O_3, $CaCl_2$, Fe_2O_3, TiO_2 and a small amount of SiO_2 [7]. The conventional landfill method leads to an accumulation of metal ions such as Ca^{2+} and Al^{3+} in the soil, threatening the health of animals, plants and humans, and causing secondary damage to the natural environment [8]. Novel RAS treatment and disposal methods with environmental and social benefits are required.

The hollow spherical AlOOH and Al_2O_3 synthesized from aluminum scrap without the use of a template, which feature a large specific surface area and total pore volume, show excellent adsorption performance for CR, with the maximum adsorption capacity of 277.00 and 478.47 mg/g, respectively, and the adsorption almost reaches equilibrium within 10 min [9]. From the aluminum slag obtained from the frame manufacturing plant, γ-Al_2O_3 can be synthesized by precipitation and calcination. It is a non-rigid aggregate of irregularly shaped particles with a plate-like structure, mesoporous structure and large surface area (304.31 $m^2 \cdot g^{-1}$). The synthetic Al_2O_3 has a high adsorption capacity for the three test dye molecules, namely, methylene blue, crystal violet and basic fuchsin, and has been shown to be superior to its commercial counterparts in terms of morphology and adsorption performance for organic dyes [10].

In this paper, RAS was modified in situ by the hydrothermal treatment of $Ca(OH)_2$ to obtain modified aluminum slag (MAS), which was used as an adsorbent. Its adsorption capacity for CR in wastewater was studied as a function of initial pH, dosage and initial concentration, and the CR adsorption mechanism

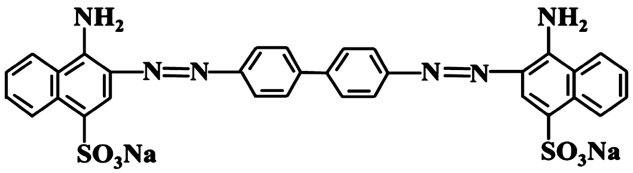

Figure 1. Chemical structural formula of CR.

was discussed.

2. Experiment

2.1. Materials

RAS for the experiment was produced by Changzhou Qingliu Environmental Protection Technology Co., Ltd. Analytical reagents (CR, hydrochloric acid, hydroxide, calcium oxide) were used in this experiment.

2.2. Experimental Procedure

2.2.1. Preparation of MAS

Firstly, 50 g RAS was weighed and put into a 500 mL beaker, into which 200 mL water was subsequently poured. Secondly, the beaker was placed on a magnetic stirrer, and the mixture was stirred. Saturated limewater was added while stirring, the pH (called initial pH) of the solution, which was continuously monitored, reached a design value (In this paper, the initial pH values were 3, 5, 7, 9, and 11, respectively). Thirdly, the mixture in the beaker was filtered using a Buchner funnel, and the filtered residue was washed twice with deionized water and then dried in a 105˚C oven. Finally, the dried residue was ground and sieved to obtain MAS.

2.2.2. MAS Adsorption Experiment on CR

Initial pH: With the initial pH of 3, 5, 7, 9, and 11, respectively, 0.3 g MAS was added to CR solutions of the same volume (V = 100 mL) and concentration (C_0 = 200 mg/L). Then, the residual CR concentration was measured after 40-min shaking in a water bath at 25˚C, and the corresponding CR residual rate was calculated.

Dosage: 0.1 g, 0.2 g, 0.3 g, 0.4 g, and 0.5 g MAS (initial pH = 7) was added to CR solutions of the same volume (V = 100 mL) and concentration (C_0 = 200 mg/L), respectively. Then, the residual CR concentration was measured after 40-min shaking in a water bath at 25˚C, and the corresponding CR residual rate was calculated. To compare the adsorption performance, 0.5 g RAS was also added to the same CR solutions as a comparative test.

Initial concentration: 0.3 g MAS (initial pH = 7) was added to CR solutions with the same volume (V = 100 mL) and different concentrations (100, 150, 200, 250, and 300 mg/L, respectively). Then, the residual CR concentration was measured after 40-min shaking in a water bath at 25˚C, and the corresponding CR residual rate was calculated.

Adsorption kinetics: 0.3 g of MAS (initial pH = 7) was added to CR solutions of equal volume (V = 100 mL) and concentration (C_0 = 200 mg/L). After shaking them in a water bath at 25˚C for 3, 5, 10, 15, 20, 30, 40, and 60 min, the supernatant was collected, the CR concentration in the solution was analyzed, and the corresponding adsorption amount was calculated.

Adsorption isotherm: 0.3 g MAS (initial pH = 7) was added to CR solutions of equal volume (V = 100 mL) and different concentrations (100, 150, 200, 250, and

300 mg/L, respectively). After shaking them in a water bath at 25˚C for 60 min, solid-liquid separation was performed, the residual CR concentration in the solution was analyzed, and the corresponding adsorption amount was calculated.

Moreover, it is important to note that the pH of all the CR solutions used in the experiment is 5, which is significantly different from the initial pH of MAS.

2.2.3. Characterization Methods

1) Material characterization

The microscopic morphology and microstructure of RAS and MAS were characterized by scanning electron micro scope (SEM), specific surface area analysis instrument (BET), X-ray diffraction (XRD) spectrometer, X-ray fluorescence (XRF) spectrometer, Fourier transform infrared (FTIR) spectrometer and zeta electric potential analyzer. In order to eliminate the influence of residual $Ca(OH)_2$, infrared spectrum analysis and XRD tests were also performed for $Ca(OH)_2$. The test equipment is as follows (**Figure 2**).

2) Adsorption performance

After the adsorption experiment, the supernatant was centrifuged and the absorbance value A of the supernatant was determined at 489 nm. The concentration C_t of residual CR in the solution was calculated using the standard curve $C_t = 73.4057A + 0.4535$, and the residual rate η was calculated with Equation (1):

$$\eta = \frac{C_t}{C_0} \tag{1}$$

where, C_0 and C_t are the mass concentration of CR in the solution before and after adsorption, respectively, mg/L.

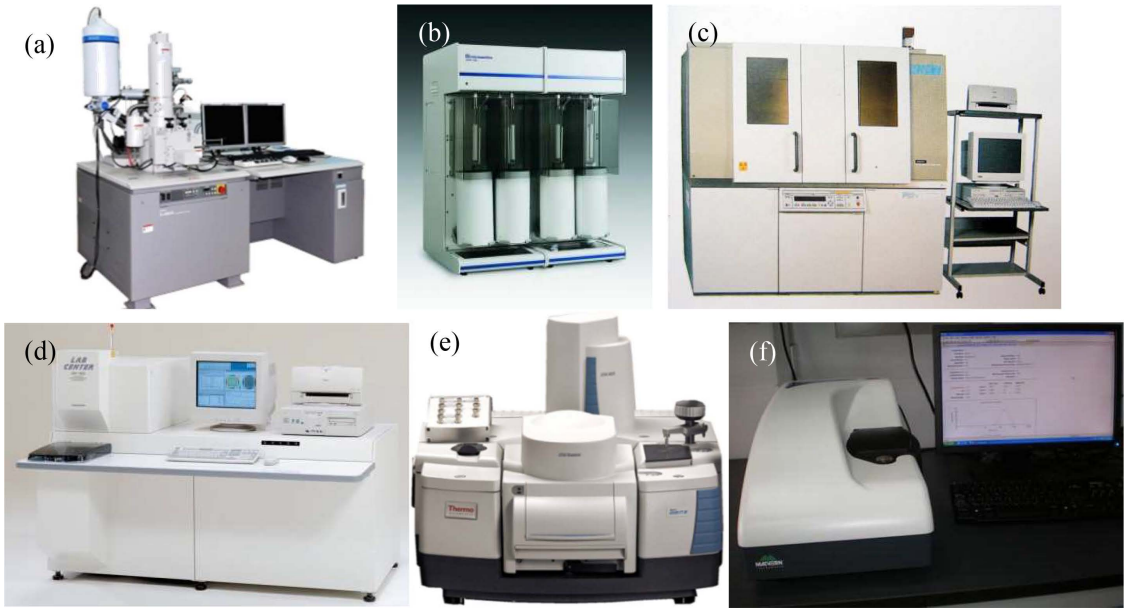

Figure 2. (a) SEM (S4800, Hitachi Manufacturing Institute, Ltd.); (b) BET (ASAP2460, McMuritik (Shanghai) Instrument Co., Ltd.); (c) XRD spectrometer (D/max2500, Nikkei Electric Co., Ltd.); (d) XRF spectrometer (XRF-1800, SHIMADZULIMITED, Japan); (e) FTIR spectrometer (iS50, Nicolet, USA); (f) Nanoparticle size and Zeta potential analyzer (Zeta size Nano ZS90, Malvern, UK).

3. Results and Discussion

3.1. Factors Affecting the Adsorption Performance of MAS for CR

3.1.1. Initial pH

Figure 3 shows the linear fitting diagram of the different pH-zeta potentials of MAS, and Figure 4 shows the removal rate of CR in wastewater by MAS with different initial pH values. It can be found from Figure 4 that the isoelectric point of MAS is 5.2. Since the isoelectric point of CR is 3.3 as reported in the literature [11], the surface of CR is positively charged when pH < 3.3 and is negatively charged when pH > 3.3. Similarly, since the isoelectric point of MAS is 5.2, the MAS surface is positively charged when pH < 5.2 but is negatively charged when pH > 5.2. Accordingly, when the solution is at a pH of 5, the surface of CR is negatively charged and the surface of MAS was positively charged while the initial pH is 3 and 5, resulting in electrostatic attractions. Because of the electric attraction and hydrogen bonds formed by the interaction of -OH in MAS and N,

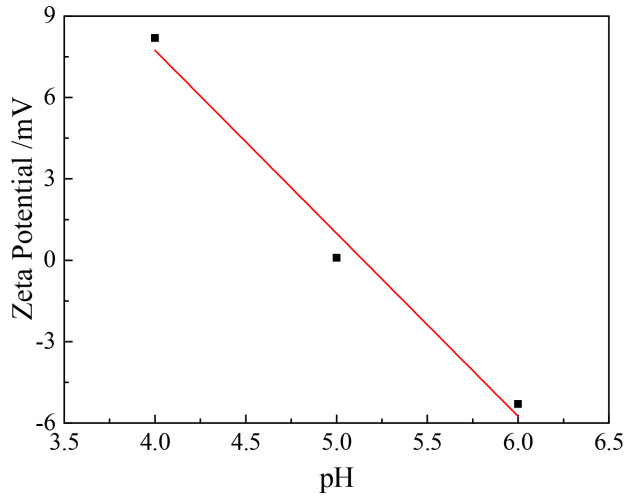

Figure 3. Linear fitting graphs of different pH-zeta potentials.

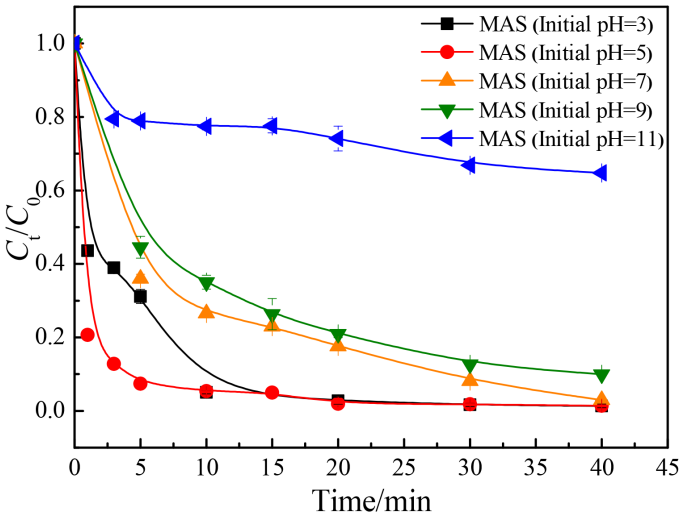

Figure 4. Removal rate of CR in wastewater by MAS under different pH.

O, S, benzene ring in CR [12], the removal performance of MAS on CR was better at initial pH of 3 and 5, with the best result at an initial pH of 5, where the removal rate of CR was 98.66% after 40 minutes of reaction.

When the initial pH was 7, 9 and 11, both the surface of MAS and CR were negatively charged. As is known to all, like charges repel each other, thus the adsorption effect of MAS on CR was not good enough when the initial pH was 7, 9 and 11.

3.1.2. Dosage

Figure 5 shows the color change of CR solution during the adsorption process. As the reaction progressing, the color of the CR solution gradually became lighter. Apparently, the adsorption performance of MAS for CR is significantly better than that of RAS.

The removal rate of CR dye effluent by MAS at different dosages is shown in Figure 6. The CR adsorption performance i is better when 0.1 g MAS is added compared with that when 0.5 g RAS is added, suggesting that it is feasible to improve the adsorption performance by slag modification. Moreover, a higher MAS dosage contributes to a higher CR removal efficiency, and a better CR adsorption performance. After 40-min reaction, the removal rate of CR reached 73.92% with an MAS dosage of 0.1 g. The C_t/C_0 curves corresponding to the MAS dosage of 0.4 g and 0.5 g essentially coincided, and the CR removal rate did not increase significantly with a further dosage increase from 0.3 g, indicating that the adsorption of MAS on CR reached a saturation state. At a dosage of 0.3 g, the CR removal rate reached 98.41% after 40-min reaction. The possible reasons are as follows: The increase in the dosage of the adsorbent allows more groups to react with CR, and therefore the unsaturated adsorption sites of the

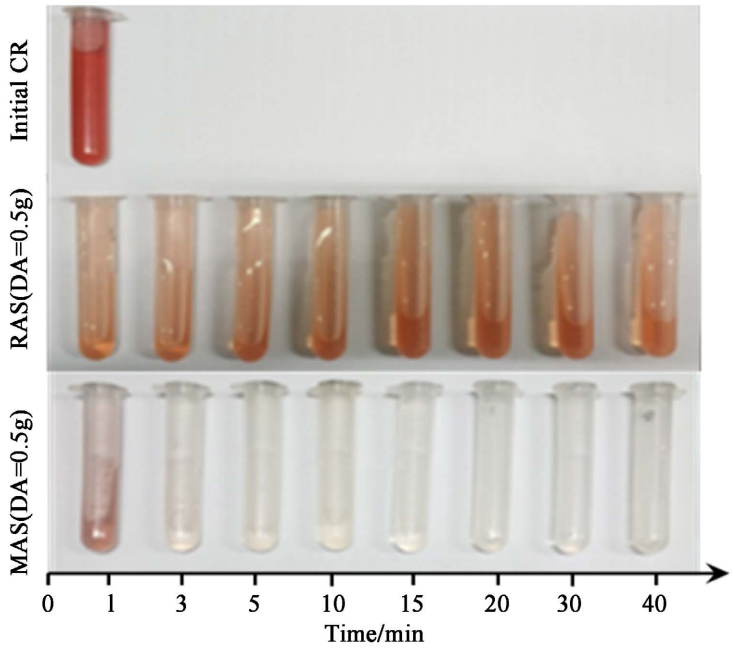

Figure 5. Color change of CR solution.

adsorbent increase [13] and the adsorption performance of the adsorbent for CR also increases. However, due to the limited CR initial concentration, the adsorption capacity of the adsorbent had exceeded the amount of CR when the dosage was increased from 0.3 g to 0.5 g.

3.1.3. Initial Concentration

The CR removal rate by MAS under different CR initial concentrations is shown in Figure 7. When the initial concentration of CR was 300 mg/L, the CR removal rate after 40-min of reaction was only 54.59%, while when the initial concentration of CR was 100 mg/L, the CR removal rate reached 98.12% after 20-min reaction, indicating that the initial concentration of CR is also an important factor affecting the CR removal rate. The changing pattern of the CR removal rate is shown in Figure 7. As the initial concentration of CR increases, the adsorption performance of MAS for CR is weakened, in other words, the increasing initial concentration of CR gradually inhibits its adsorption performance of MAS.

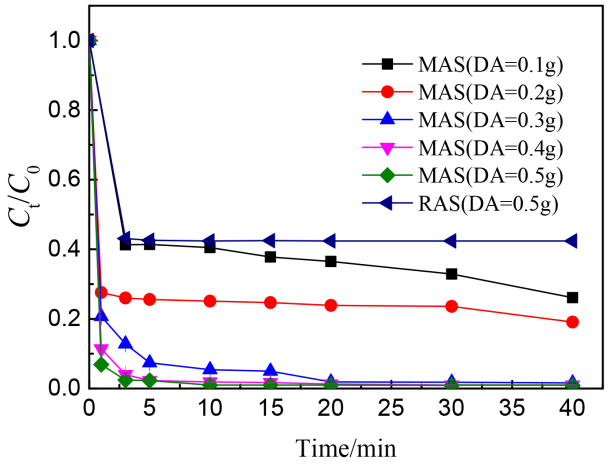

Figure 6. The effect of dosage on the removal of CR by MAS.

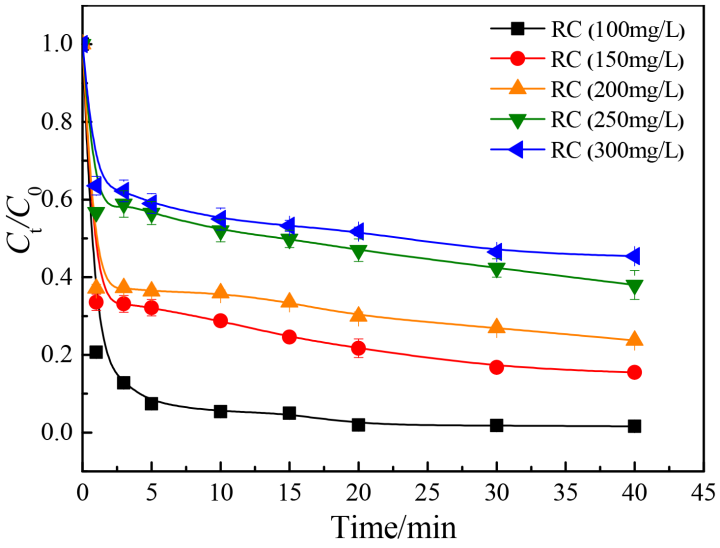

Figure 7. CR removal rate by MAS under different initial CR concentrations.

3.1.4. Adsorption Kinetics

The adsorption kinetic data of CR in wastewater are shown in Figure 8. It can be seen that the adsorption was very fast before 20 min, and after 40 min the adsorption became very slow, indicating that the adsorption of CR reached a steady state, and the equilibrium adsorption capacity is 37.713 $mg \cdot g^{-1}$.

The adsorption kinetics is usually described by Lagergren's first-order kinetics model and second-order kinetics model, as shown in Equation (2) and Equation (3), respectively [14]:

$$\lg\left(q_e - q_t\right) = \lg q_e - \frac{k_1}{2.303}t \tag{2}$$

$$\frac{t}{q_t} = \frac{1}{k_2 q_e^2} + \frac{1}{q_e}t \tag{3}$$

where q_e and q_t represent the adsorption capacity at equilibrium and at time t, respectively, in $mg \cdot g^{-1}$; k_1 and k_2 represent the Lagergren first-order and second-order adsorption rate constants, in $L \cdot min^{-1}$ and $g \cdot mg^{-1} \cdot min^{-1}$ respectively.

The parameters of the kinetic adsorption model were determined by linear regression by substituting the data in Figure 8 into Equation (2) and Equation (3), respectively. The regression parameters are shown in Table 1. From Table 1, it can be seen that the CR adsorption behavior of MAS on CR conforms to the second-order kinetic model, as the linear correlation coefficient R_2 of the second-order kinetic model is 0.999.

3.1.5. Analysis of Internal Diffusion Mechanism of Adsorption

Weber-Morris model is a dynamic model describing the diffusion process of

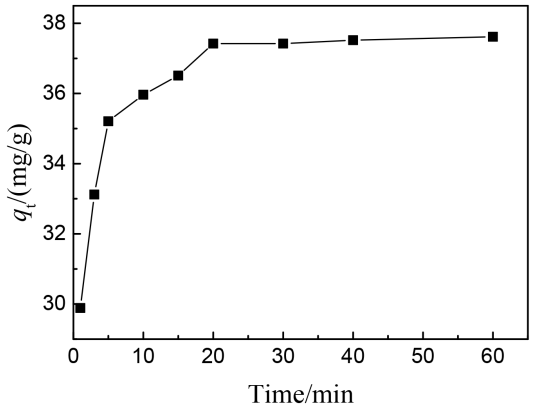

Figure 8. Adsorption performance of MAS for CR at different time.

Table 1. Parameters of adsorption kinetic model of MAS for CR.

Adsorbent	q_e/ ($mg \cdot g^{-1}$)	Lagergren first-order dynamics			Secondary dynamics		
		k_1/ ($L \cdot min^{-1}$)	$q_{e,c}$/ ($mg \cdot g^{-1}$)	R_2	k_2/ ($g \cdot mg^{-1} \cdot min^{-1}$)	$q_{e,c}$/ ($mg \cdot g^{-1}$)	R_2
MAS	37.713	0.0608	22.342	0.788	0.0611	37.893	0.999

pollutant molecules. In this paper, it was used to fit the test data. The Weber-Morris internal diffusion model is shown in Equation (4) [15]:

$$q_t = K_i t^{1/2} + C \tag{4}$$

where q_t is the adsorption capacity at time t in mg·g^{-1}; K_i is the adsorption coefficient of the internal diffusion model in mg·g^{-1}·min$^{-0.5}$; C is the thickness constant of the boundary layer on the surface of the adsorbent in mg·g^{-1}.

Based on the kinetic adsorption data from **Figure 8**, the CR adsorption capacity was calculated by the piecewise fitting method using Equation (4), and the results are shown in **Figure 9** and **Table 2**.

From **Figure 9**, it can be seen that the adsorption of CR by MAS is divided into a membrane diffusion process (K_1), an internal diffusion process (K_2) and an adsorption equilibrium process (K_3). In the first phase, the molecules of CR pass through the film of the liquid medium adhering to the surface of the adsorbent and reach the outer surface of the adsorbent from the liquid phase. In the second phase, the CR molecules on the outer surface gradually pass through the pores in the adsorbents and reach its inner surface. In the third phase, the CR molecules reach the adsorption site on the inner surface of the adsorbent and accumulate, and therefore the adsorption equilibrium state is quickly reached.

The parameters of the Weber-Morris model were obtained by piecewise fitting (see **Table 2**). $K_1 > K_2 > K_3$ indicates that the adsorption rate of the membrane diffusion process is the fastest, the internal diffusion process is second, and the adsorption rate in the adsorption equilibrium process is the slowest. The modification

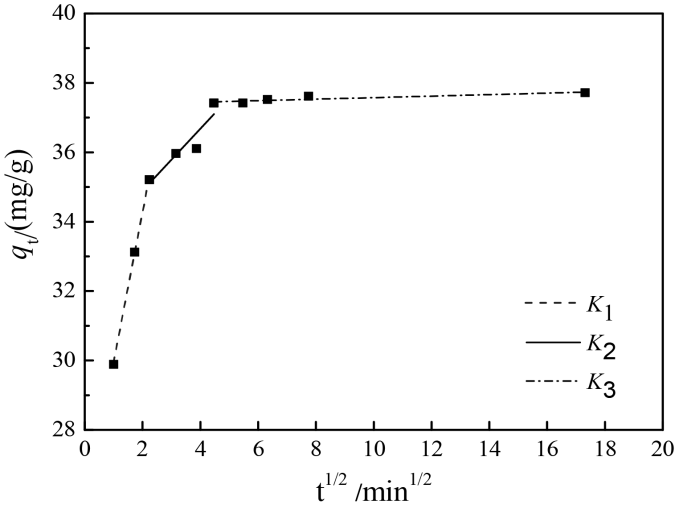

Figure 9. Weber-Morris internal diffusion model equation for CR adsorption by MAS.

Table 2. Weber-Morris kinetic constants for CR-MAS adsorption.

Weber-Morris internal diffusion model parameters	K_1/ mg·g^{-1}·min$^{-0.5}$	R^2	K^2/ mg·g^{-1}·min$^{-0.5}$	R^2	K^3/ mg·g^{-1}·min$^{-0.5}$	R^2
Fitting value	4.315	1.00	0.893	0.808	0.022	0.725

greatly improved the roughness and specific surface area of RAS, maintaining the initial adsorption rate at a high level. However, the internal diffusion process started and the adsorption rate slowed down over time due to the clogging of the internal channels of the adsorbent. In the adsorption equilibrium process, the adsorption rate was almost 0. In addition, since the fitted equation in the internal diffusion process did not pass through the origin, the adsorption rate of CR by MAS was determined by the interaction of membrane diffusion and internal diffusion.

3.1.6. Adsorption Isotherm

The isothermal adsorption equation is of great significance and an effective means in the study of solute transport, especially the transport of pollutants in the geological environment. In this paper, the relationship between the CR adsorption amount per unit mass of MAS and t residual CR was studied based on the adsorption isotherm.

After 60-min of shaking in a water bath at 25˚C, the adsorption capacity of MAS for CR in solutions with different CR concentrations is shown in **Figure 10**. It can be seen that the adsorption capacity of MAS for CR is enhanced with the increase of the initial concentration of CR solution.

The experimental data were fitted by Langmuir adsorption isotherm [16] and Freundlich adsorption isotherm [17].

Langmuir adsorption isotherm is shown in formula (5):

$$\frac{t}{q_e} = \frac{1}{Q_0} + \left(\frac{1}{bQ_0}\right)\left(\frac{1}{C_e}\right) \tag{5}$$

Freundlich adsorption isotherm is shown in formula (6):

$$\lg q_e = \lg K + \frac{1}{n}\lg C_e \tag{6}$$

where, q_e is the amount of adsorbate per unit mass of adsorbent in mg·g^{-1}; C_e is the residual adsorbate in the solution at equilibrium in mg/L; Q_0 is the saturated adsorption capacity per unit mass of adsorbent when the monolayer is formed in

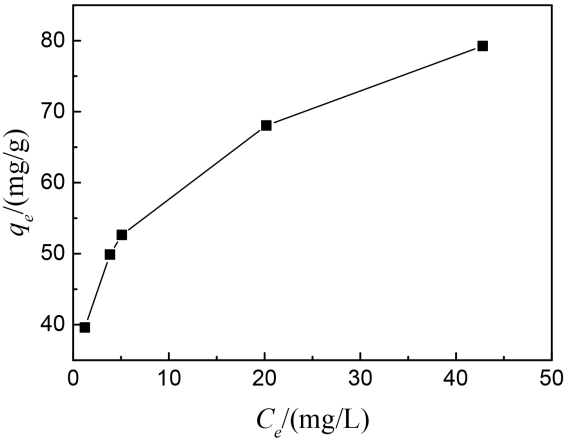

Figure 10. Adsorption isotherm of MAS for CR.

$mg \cdot g^{-1}$; b and K are constants in $L \cdot mg^{-1}$; n is a constant related to temperature and other factors. The regression parameters are shown in Table 3.

It can be seen from Table 3 that the CR adsorption behavior of MAS conforms to the Freundlich adsorption isotherm equation, therefore, the adsorption of CR by MAS belongs to multilayer adsorption.

3.2. MAS Characterization Analysis

3.2.1. FTIR Analysis

The FTIR diagrams of RAS (before/after reaction, BR/AR), MAS (BR/AR) and $Ca(OH)_2$ are shown in Figure 11. As shown in Figure 11(a), there are five absorption bands in the infrared spectrum, and the difference between the absorption bands of MAS and $Ca(OH)_2$ is significant, which proves that there is no residual $Ca(OH)_2$ in MAS. It can also be found that the distribution of the infrared spectrum of MAS remains unchanged due to the use of $Ca(OH)_2$ for modification, indicating that the modification does not change the main functional groups of the aluminum slag. The absorption bands around 3640 cm^{-1}, 1460 cm^{-1}, 1010 cm^{-1}, 529 cm^{-1} and 402 cm^{-1} are associated with the stretching vibration of M-OH in calcium oxide, the bending vibration of -OH, the stretching vibration of Si-O-Fe or Si-O-Al, the stretching vibration of Al-O and Fe-O and the inverse stretching vibration of Al-O and Fe-O, respectively. A comparison of Figure 11(a) and Figure 11(b) shows that the position of the absorption band of the infrared spectrum of MAS or RAS did not change significantly before and after adsorption, which is due to the low initial concentration of CR.

Table 3. Isothermal parameters of adsorption by MAS.

Adsorbent	Langmuir isotherm parameters			Freundlich isotherm parameters		
	Q_0/mg·g^{-1}	b/L·mg^{-1}	R_2	K/L·mg^{-1}	n	R_2
MAS	10.41	60.04	0.874	38.24	5.16	0.999

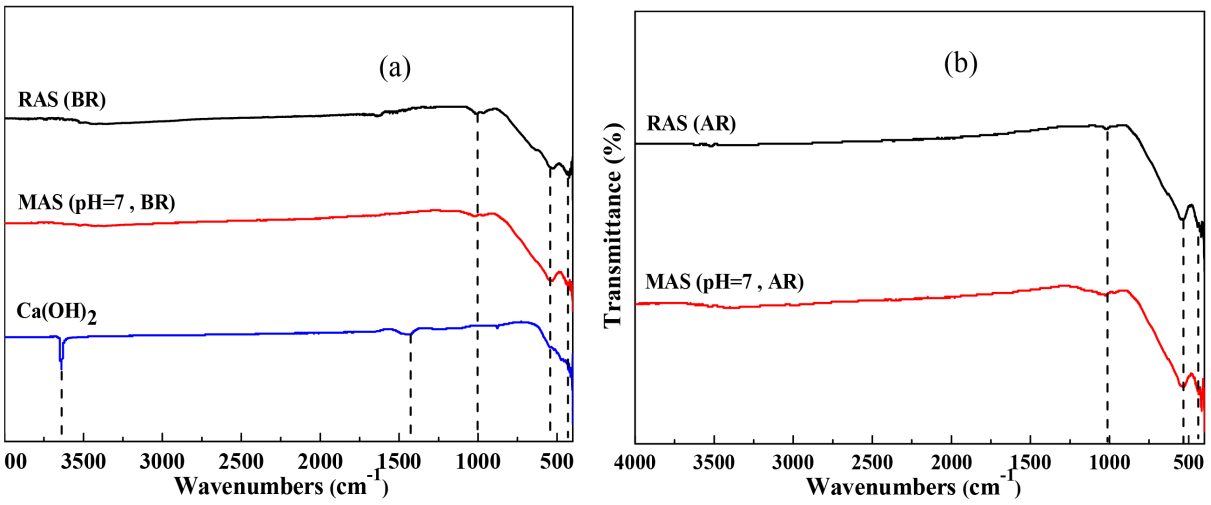

Figure 11. (a) FTIR diagrams of RAS, MAS (BR) and $Ca(OH)_2$; (b) FTIR diagrams of RAS, MAS (AR).

3.2.2. XPS Analysis

To investigate the effect of the constituents on the adsorption behavior, XPS analysis was performed for some MAS samples, and the XPS diagram is shown in Figure 12. According to the test results, the content of Fe (II) reaches 45.52%. The results of previous research show that coordination interaction between Fe (II) and CR molecules allows CR molecules to flocculate and be adsorbed in neutral and alkaline environments [18].

3.2.3. XRD Analysis

The XRD patterns of RAS (BR), MAS (BR) and $Ca(OH)_2$ are shown in Figure 13.

At 2θ = 18.040˚, 32.830˚, 36.593˚, 47.270˚, 58.996˚ and 64.772˚, both the diffraction of RAS (BR) and of MAS (BR) show sharp diffraction peaks, and at 2θ = 18.040˚, 28.804˚, 34.142˚, 47.182˚, 50.945˚, 54.358˚, 62.672˚, 64.422˚, 71.949˚, the diffraction of $Ca(OH)_2$ generally shows sharp diffraction peaks. Through pattern recognition with MDI Jade 6.0 software, these diffraction peaks were found to correspond to the standard PDF maps of $Ca(OH)_2$, $CaTiO_3$, $FeAl_2O_4$

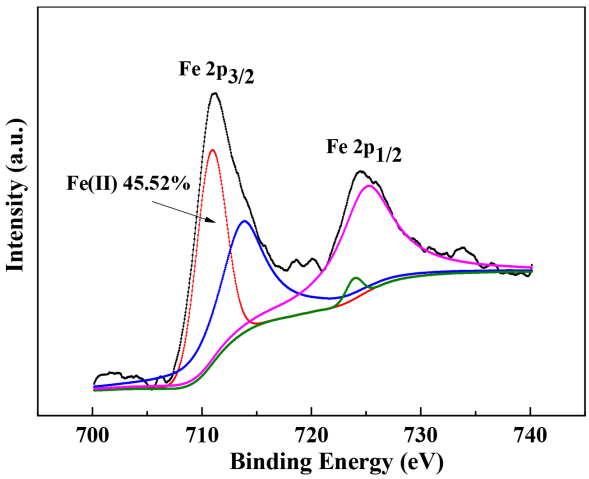

Figure 12. XPS spectrum of MAS.

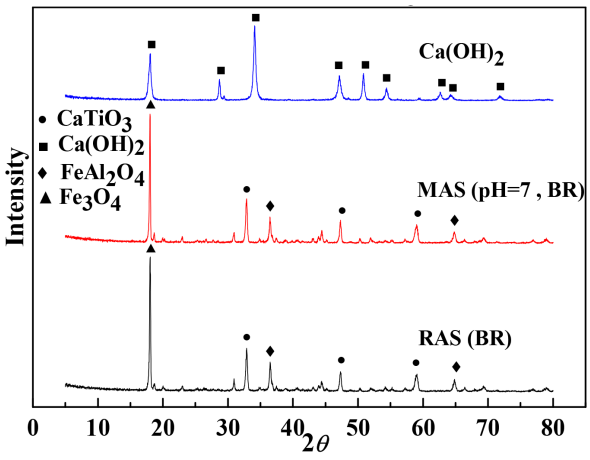

Figure 13. XRD patterns of RAS (BR), MAS (BR) and $Ca(OH)_2$.

and Fe_3O_4, respectively. Combing the results of infrared spectroscopy analysis, we can conclude that the main components of RAS are calcium-titanium oxide, iron-alumina oxide and iron trioxide, and the chemical components of RAS have not been damaged during the modification process due to the good crystalline phase. According to previous studies [19], Fe_3O_4 has a strong adsorption capacity for CR.

3.2.4. BET Analysis

N_2 adsorption was carried out for the samples MAS and RAS to evaluate the permanent porosity. The results are shown in **Figure 14(a)**, **Figure 14(b)** and **Table 4**. From **Figure 14(a)**, it can be seen that both MAS and RAS exhibit an irreversible isotherm of the IV type, which is one of the main characteristics of mesoporous materials. From the combination of **Figure 14(b)** and **Table 4**, it can be seen that the pore volume and specific surface area of MAS are 0.033162 $cm^3 \cdot g^{-1}$ and 16.3308 $m^2 \cdot g^{-1}$, which are 3.48 and 3.91 times of the value before modification, respectively. This is the main reason why the CR adsorption capacity of MAS can be significantly improved.

3.2.5. SEM Analysis

The SEM images of RAS and MAS are shown in **Figure 15**. After modification with $Ca(OH)_2$, some $Ca(OH)_2$ enters the aluminum slag, which changes the original morphology of the aluminum slag and disperses the aggregates, which explains why MAS has a rougher surface, a looser pore structure and a larger specific surface area. The changed morphology of MAS favors its dispersion in

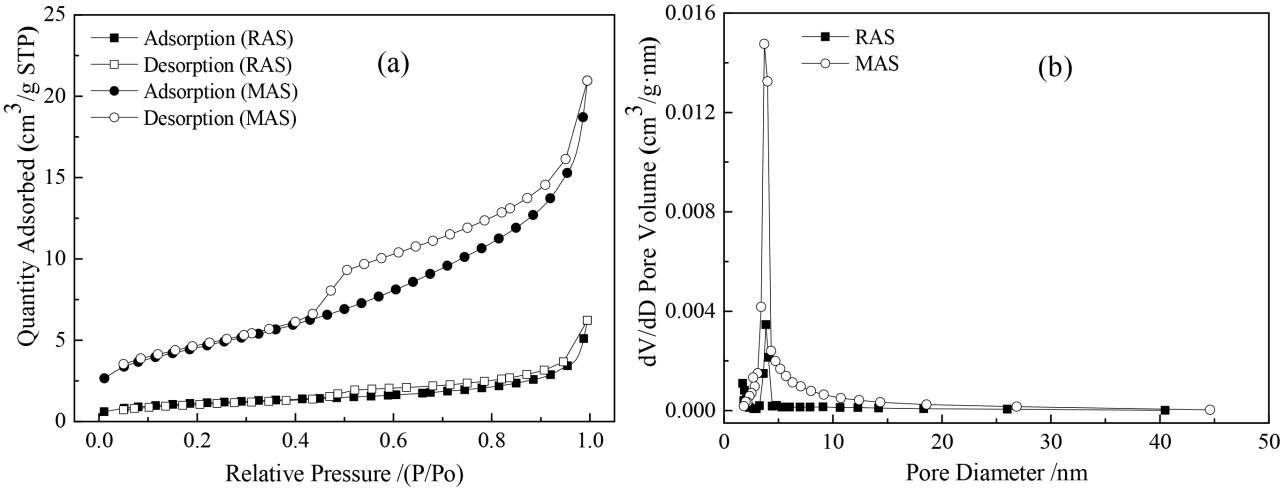

Figure 14. (a) Adsorption-desorption isotherm; (b) Pore size distribution of RAS and MAS.

Table 4. Specific surface and pore size characteristics of RAS and MAS.

Material	Specific surface area $m^2 \cdot g^{-1}$	Pore size nm	Pore volume $cm^3 \cdot g^{-1}$
RAS	4.1820	10.1113	0.009529
MAS	16.3308	7.0081	0.033162

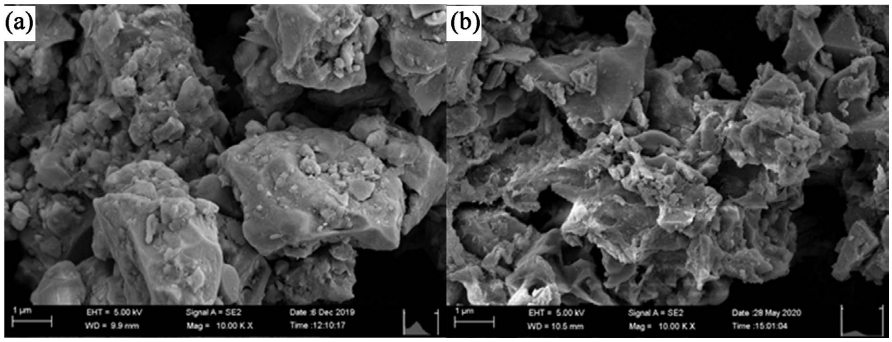

Figure 15. SEM patterns of RAS and MAS [(a) RAS; (b) MAS].

wastewater, and the looser pore structure of MAS makes it easier for CR to reach its inner surface. Furthermore, a larger specific surface area improves the adsorption of CR. Besides the larger specific surface area, finer MAS particles also play a role in electrical neutralization and adsorption bridging. It can be summarized that the microstructure of MAS improves its CR removal efficiency.

4. Conclusions

In this research, MAS was used as an adsorbent for CR, a series of single-factor tests were carried out. In addition, the structure and morphology of RAS and MAS were characterized by FTIR, XPS, XRD, BET and SEM. The results show that:

1) MAS exhibits excellent adsorption behavior for CR. At 25˚C, with an MAS dosage of 0.3 g, initial concentration of CR of 100 mg/L, initial pH of 5, and adsorption time of 40 min, the removal rate of CR is 98.41%.

2) The adsorption behavior of MAS for CR conforms to second-order kinetics, and the adsorption isotherm follows the Freundlich isotherm model. In the Weber-Morris internal diffusion equation, $K_1 > K_2 > K_3$, indicating that the adsorption rate is determined by the interaction of membrane diffusion and internal diffusion, and in the membrane diffusion process, the fastest adsorption rate is the fastest.

3) FTIR and XRD analysis shows that the main chemical constituents of MAS are calcium titanium oxide, iron aluminum oxide and iron trioxide with good chemical stability, and XPS analysis confirms that the Fe (II) reaches 45.52%.

4) After the modification by the hydrothermal treatment of $Ca(OH)_2$, MAS shows higher porosity and a larger specific surface area. The pore volume and specific surface area of MAS were 3.48 and 3.91 times higher than the value before modification, contributing to its rougher surface and looser pore structure.

Acknowledgements

The support of General projects with joint special funds for basic research of Local Undergraduate Universities in Yunnan Province (Grant No. 202101BA070001-080) and Talent Introduction Project of Kunming University (Grant No. YJL20026). The work of this paper is also supported by the following projects: Frontier Re-

search Team of Kunming University 2023.

Conflicts of Interest

The authors declare no conflicts of interest regarding the publication of this paper.

References

[1] Shabana, N., Arjun, A.M., Ankitha, M., *et al.* (2023) $Nb_2CTx@MoS_2$ Composite as a Highly Efficient Catalyst for the Degradation of Organic Dyes. *Catalysis Communications*, **173**, Article ID: 106566. https://doi.org/10.1016/j.catcom.2022.106566

[2] Shabnam, R., Miah, M.A.J., Sharafat, M.K., *et al.* (2019) Cumulative Effect of Hydrophobic PLMA and Surface Epoxide Groups in Composite Polymer Particles on Adsorption Behavior of Congo Red and Direct Red-75. *Arabian Journal of Chemistry*, **12**, 4989-4999. https://doi.org/10.1016/j.arabjc.2016.10.016

[3] Alsamhary, K., Al-Enazi, N.M., Alhomaidi, E., *et al.* (2022) *Spirulina platensis* Mediated Biosynthesis of Cuo Nps and Photocatalytic Degradation of Toxic Azo Dye Congo Red and Kinetic Studies. *Environmental Research*, **207**, Article ID: 112172. https://doi.org/10.1016/j.envres.2021.112172

[4] Wang, X., Deng, B., Yu, L., *et al.* (2020) Degradation of Azo Dyes Congo Red by MnBi Alloy Powders: Performance, Kinetics and Mechanism. *Materials Chemistry and Physics*, **251**, Article ID: 123096. https://doi.org/10.1016/j.matchemphys.2020.123096

[5] Sathishkumar, K., Alsalhi, M.S., Sanganyado, E., *et al.* (2019) Sequential Electrochemical Oxidation and Bio-Treatment of the Azo Dye Congo Red and Textile Effluent. *Journal of Photochemistry and Photobiology B*: *Biology*, **200**, Article ID: 111655. https://doi.org/10.1016/j.jphotobiol.2019.111655

[6] Subbaiah Munagapati, V., Wen, H.-Y., Gollakota, A.R.K., *et al.* (2022) Magnetic Fe_3O_4 Nanoparticles Loaded Papaya (*Carica papaya* L.) Seed Powder as an Effective and Recyclable Adsorbent Material for the Separation of Anionic Azo Dye (Congo Red) from Liquid Phase: Evaluation of Adsorption Properties. *Journal of Molecular Liquids*, **345**, Article ID: 118255. https://doi.org/10.1016/j.molliq.2021.118255

[7] Shen, H., Liu, B., Shi, Z., *et al.* (2021) Reduction for Heavy Metals in Pickling Sludge with Aluminum Nitride in Secondary Aluminum Dross by Pyrometallurgy, Followed by Glass Ceramics Manufacture. *Journal of Hazardous Materials*, **418**, Article ID: 126331. https://doi.org/10.1016/j.jhazmat.2021.126331

[8] Shen, H., Liu, B., Ekberg, C., *et al.* (2021) Harmless Disposal and Resource Utilization for Secondary Aluminum Dross: A Review. *Science of the Total Environment*, **760**, Article ID: 143968. https://doi.org/10.1016/j.scitotenv.2020.143968

[9] Guo, J., Shen, X., Shao, H., *et al.* (2022) Facile and Template-Free Fabrication of Hollow Spherical AlOOH and Al_2O_3 from the Waste Aluminum Residue: Growth Mechanism and Fast Removal of Congo Red. *Journal of Solid State Chemistry*, **316**, Article ID: 123627. https://doi.org/10.1016/j.jssc.2022.123627

[10] Fernandes, E.P., Silva, T.S., Carvalho, C.M., *et al.* (2021) Efficient Adsorption of Dyes by γ-Alumina Synthesized from Aluminum Wastes: Kinetics, Isotherms, Thermodynamics and Toxicity Assessment. *Journal of Environmental Chemical Engineering*, **9**, Article ID: 106198. https://doi.org/10.1016/j.jece.2021.106198

[11] Amalina, F., Abd Razak, A.S., Krishnan, S., *et al.* (2022) A Review of Eco-Sustainable Techniques for the Removal of Rhodamine B Dye Utilizing Biomass Residue Ad-

sorbents. *Physics and Chemistry of the Earth, Parts A/B/C*, **128**, Article ID: 103267. https://doi.org/10.1016/j.pce.2022.103267

[12] Wu, Z., Yuan, X., Zhong, H., *et al.* (2017) Highly Efficient Adsorption of Congo Red in Single and Binary Water with Cationic Dyes by Reduced Graphene Oxide Decorated NH_2-MIL-68(Al). *Journal of Molecular Liquids*, **247**, 215-229. https://doi.org/10.1016/j.molliq.2017.09.112

[13] Wang, H., Yang, L., Qin, Y., *et al.* (2023) Highly Effective Removal of Methylene Blue from Wastewater by Modified Hydroxyl Groups Materials: Adsorption Performance and Mechanisms. *Colloids and Surfaces A*: *Physicochemical and Engineering Aspects*, **656**, Article ID: 130290. https://doi.org/10.1016/j.colsurfa.2022.130290

[14] Li, Y., Yang, Y., Qu, G., *et al.* (2022) Reuse of Secondary Aluminum Ash: Study on Removal of Fluoride from Industrial Wastewater by Mesoporous Alumina Modified with Citric Acid. *Environmental Technology & Innovation*, **28**, Article ID: 102868. https://doi.org/10.1016/j.eti.2022.102868

[15] Zhu, Q., Moggridge, G.D. and D'agostino, C. (2016) Adsorption of Pyridine from Aqueous Solutions by Polymeric Adsorbents MN 200 and MN 500. Part 2: Kinetics and Diffusion Analysis. *Chemical Engineering Journal*, **306**, 1223-1233. https://doi.org/10.1016/j.cej.2016.07.087

[16] Guo, X. and Wang, J. (2019) Comparison of Linearization Methods for Modeling the Langmuir Adsorption Isotherm. *Journal of Molecular Liquids*, **296**, Article ID: 111850. https://doi.org/10.1016/j.molliq.2019.111850

[17] Ezzati, R. (2020) Derivation of Pseudo-First-Order, Pseudo-Second-Order and Modified Pseudo-First-Order Rate Equations from Langmuir and Freundlich Isotherms for Adsorption. *Chemical Engineering Journal*, **392**, Article ID: 123705. https://doi.org/10.1016/j.cej.2019.123705

[18] Azha, S.F., Sellaoui, L., Engku Yunus, E.H., *et al.* (2019) Iron-Modified Composite Adsorbent Coating for Azo Dye Removal and Its Regeneration by Photo-Fenton Process: Synthesis, Characterization and Adsorption Mechanism Interpretation. *Chemical Engineering Journal*, **361**, 31-40. https://doi.org/10.1016/j.cej.2018.12.050

[19] Wang, L., Yu, Y. and Yao, W. (2017) Preparation of Nanocrystalline Fe_3O_4 and Study on Their Adsorption Performance for Congo Red. *Inorganic Chemicals Industry*, **49**, 37-40.